Microsc. Microanal. Microstruct. **5** (1994) 213–236 JUNE **1994**, PAGE 213

Classification
Physics Abstracts
73.61J — 61.43D — 68.65 — 61.16B — 64.75

Analysis of MBE growth and atomic exchange in thin highly strained InAs layers

C. d'Anterroches([1]) and J.M. Gerard([2])

([1]) France Télécom CNET, BP. 98, 38243 Meylan, France
([2]) France Télécom CNET, 196, avenue H. Ravera, 92220 Bagneux, France

(Received June 17; accepted September 26, 1994)

Résumé. — L'objet de ce travail est de prouver l'existence d'une ségrégation de l'indium lors de la croissance de GaAs sur un film d'InAs, et de trouver une technique pour l'éviter. Pour cela les films contraints de InAs/GaAs ont été obtenus dans différentes conditions de croissance, des films isolés, des multicouches et des multipuits quantiques ont été étudiés. Des images de microscopie électronique haute résolution en transmission ont été analysées en détail afin de déterminer le meilleur moyen pour clairement différencier indium et gallium. La comparaison des résultats obtenus en faisant des simulations d'images, des mesures de distortion et des mesures d'intensité ont montré que les mesures d'intensité sont les plus sensibles pour l'analyse de l'indium. Moins de 6% d'indium peut être détecté. Les résultats obtenus par cette technique ont été complétés par l'étude des propriétés optiques des films. Il a été démontré que la distribution d'indium au delà d'une monocouche est due à une ségrégation en surface lors de la croissance, et qu'une technique de prédéposition permet de l'éviter.

Abstract. — The aim of this work is to prove the segregation process of indium during the growth of GaAs on InAs layers. A variety of structures has been grown to allow us to determine the width of indium distribution according to the growth process. Strained InAs/GaAs films as monolalayers, multilayers or multiquantum wells have been obtained. The indium segregation during growth has been proved in analyzing the electron images of the films and a new method for avoiding indium segregation in InGaAs/GaAs superlattices has been developed. Concerning the detailed image analyzis using image simulation, distortion measurements and intensity measurements have shown that intensity measurement is the most sensitive way to detect InAs containing layers in a GaAs matrix. It is demonstrated that less than 6% of indium can be detected. The segregation process has been demonstrated on symmetrical structures, and the nominal position of indium was determined with reference to AlAs films. Furthermore, a novel technique, which, by predeposition of indium, controls the segregation itself in order to build abrupt interfaces in the InGaAs/GaAs system, has been validated.

1. Introduction.

High quality semiconductors can now be built into complex structures such as quantum wells, superlattices or graded heterojunctions. The quality of the stuctures themselves is illustrated in

GaAs/GaAlAs superlattices where the barrier/well interfaces are atomically flat over distances of up to 100 nm and accuracies on the well width of one atomic layer have been claimed [1]. To a certain extent, this advanced state of the art is also true for strained heterostructures. As long as the lattice mismatch does not exceed one per cent typically, a nearly ideal two-dimensional growth mode is preserved for the strained layers. The single essential limitation for these "weakly" strained structures is the well-known existence of a critical thickness for the epilayer (if it is strained as a whole with respect to the substrate), over which plastic relaxation is favorable from the energy point of view. In contrast, the growth of highly strained layers remains particularly challenging at present, due to the strong influence of a large lattice mismatch on the growth mode of the epilayer. For the most important highly strained systems such as Ge/Si [1, 2] or InAs/GaAs [3, 6] a Stranski-Krastanov growth mode can be observed under standard MBE growth conditions: the growth proceeds first bidimensionally (2D growth), but 3D islands nucleate on this 2D wetting layer once the thickness of the strained epilayer exceeds a certain critical thickness in the few monolayer (ML) range. A 3D morphology is now energetically favored since it permits an efficient relaxation of the highly strained material. Considerable efforts have also been devoted to the suppression of this -generally undesirable- morphology change, with some success for certain approaches (codeposition of surfactant species [7, 8], low temperature growth [5], use of special growth techniques such as MBE assisted by ion bombardement [9] or migration enhanced epitaxy [10, 11]). On the other hand potentially useful heterostructures can also be grown when keeping the individual thickness of each highly strained layer below its critical thickness, including ultrathin strained quantum well layers in an unstrained matrix (such as InAs in GaAs [3]) and short period superlattices formed by alternate layers under strong biaxial tension or compression (such as InAs/GaAs [10-12, 13] or InAs/AlAs [11] on InP). For such structures, at least partially built with very thin layers, the structural perfection is however intrinsically limited by surface segregation processes, as shown for numerous systems, including InAs/GaAs [14, 15], Si/Ge [16] and even (to a lesser extent) the unstrained GaAs/AlAs system [14, 15].

HREM allows atomic probing, and the limit of this technique is to differenciate two materials showing very similar structures. This is the case in InAs/GaAs heterostructures. To analyze the image contrast, one can take into account the difference in dynamic interaction between the incident electron beam and the two crystals InAs and GaAs respectively. Moreover as there is a large lattice mismatch between them, the strain field can be demonstrated by measuring the lattice distortion. Finally, the diffusion contrast allows the indium and gallium to be localized. To interpret HREM images these three methods have been used in this work, as will be shown below. Moreover it is shown how this technique is enriched by association with other analytical techniques, mainly optical ones used for analysing the InAs growth.

2. Technical descriptions.

The multilayers studied in this work were grown on GaAs (001) by either conventional molecular beam epitaxy (MBE) (CL4, CL5, CL2a) or migration-enhanced epitaxy (MMBE) (ML1, ML2, CL2b, CL3). Two others (CL1, CL6) were grown on InP (001) by MBE.

They were grown as the following. First: an 0.9 ML QW (ML1) and a 1.7 ML QW (ML2) were studied in order to analyze the structure evolution when passing from 2D to 3D growth. Secondly short periodicity multilayers grown on InP were analyzed. Then the efficiency of migration-enhanced epitaxy has been proved for the growth of $(InAs)_2/(GaAs)_2$ (CL2b) and $(InAs)_3/(GaAs)_3$ (CL3) multilayers, and a technique allowing control of the indium profile was obtained for $In_{0.11}Ga_{0.89}As/GaAs$ (CL1, CL6). The segregation process was demonstrated on two symmetrical heterostructures (CL4 and CL5).

The MBE growth has been described by L. Golstein *et al.* [3]: it was performed at 550 °C under As-stabilized conditions in order to optimize the quality of the whole structure.

The MMBE growth has been described by J.M. Gerard *et al.* [10]. After growth of a 0.5 μm thick GaAs buffer layer by standard MBE, the substrate temperature was lowered to 350 °C during a growth interruption; then column III species and As_4 molecules were alternately sent to the sample.

The growth process was monitored on-line by high energy electron diffraction (RHEED) and the average film thickness could therefore be determined. The thickness measurement was confirmed using the X-Ray double diffraction technique [21] assuming a tetragonal distortion of the InAs film as predicted by the continuum elasticity theory. However, this is only an approximation, given that the GaAs surface is not exactly flat as it will be shown later and there is a rhombohedral distortion as described in the work of C. d'Anterroches *et al.* [22].

For the electron microscopy study, cross-section samples were prepared by sticking pieces of wafer together and mechanically polishing them. Subsequent conventional ion-milling from both sides (Ar^+, 5 kV, 0.5 mÅ, 15° angle of incidence) was applied to obtain perforation [22].

Microscopy was performed using a JEOL 200 CX operating at 200 kV, with an aperture of 7 nm^{-1} diameter and a Scherzer defocus value ($\Delta f = 60$ nm).

Three methods, described below, were used to interpret the high resolution images.

a) To understand the contrast obtained in HREM, dynamical calculations were performed using Stadelmann's EMS programs [23]. These offer two methods for calculation of the wavefunction at the exit face of a crystal slab: the fast Fourier transform-based "multislice" method and the Bloch formalism. The multislice method was used to simulate the InAs/GaAs interface contrast while the Bloch formalism enabled us to calculate the amplitude and phases of the preponderant beams in the perfect crystal. The interaction of the electron beam with AlAs, GaAs and InAs respectively was compared.

b) Micrographs were digitized to evaluate the mean value of the atomic column intensity. The film thickness, during the growth process, is measured in number of monolayers. One monolayer is $\frac{1}{2}$ [001] a thick, this is half the crystal periodicity. The intensity mean value over one monolayer is an average of the atomic projection column and hole intensity.

c) Digitized micrographs were also analyzed in terms of local lattice distortion measurements. This method has been proposed previously by using a vernier-effect directly on the image [22]. This applies to the InAs/GaAs system as the lattice mismatch is large: about 7%. A mathematical method has recently been proposed [24]. A detailed description of the method used in this work is given by P.H. Jouneau *et al.* [25]. Briefly, the positions of all maxima in the digitized images are determined accurately. To obtain a position precision greater than one pixel, the dot position is determined from calculation of the center of mass of the intensity profile. A reference area is chosen in the undisturbed region to measure the displacements between the ideal lattice and the strained lattice. The results is given after averaging along one layer in the direction perpendicular to the growth.

3. Sensitivity limit of indium detection.

High resolution images result from the dynamic interaction between the incident electron beam and the crystal. The multibeam theory has been introduced to solve this problem. It shows that the image contrast depends on both the dynamic amplitudes and the phases of the diffracted electron beams. The dynamic amplitude calculated according to the Howie and Whelan theory is proportional to the structure factor.

The materials studied in this work exhibit the sphalerite structure; for this structure two zone axes are used to achieve the HREM imaging, that is the [100] and [110] directions. In these directions the preponderant interacting beams are {022} and {111} respectively, and for both {200}.

It would be interesting to be able to differentiate the crystals by their respective beam behavior. It is well known [26] that, for the studied structure, the preponderant beams in the image are the {111} beams along the [011] beam axis and the {022} beams along the [100] beam axis. Their behavior has been analyzed in detail by S. Thoma *et al.* [27] in order to apply the so-called "chemical lattice imaging" [28] to the AlAs/GaAs multilayers. The method works very well for distinguishing between GaAs and AlAs films but unfortunately cannot be used to differentiate GaAs an InAs films as explained below.

The contrast variation results from competition between the {200} beams and the {220} or {111} beams. Provided the illumination is coherent, only the dynamic amplitudes [27] U_{020}. U_{220} or U_{200}, U_{111}, and relative phases φ_{020}, φ_{220} or φ_{200}, φ_{111} must be determined as a function of sample thickness by executing a numerical Bloch wave calculation. The image intensity of the reciprocal vector **g** is given by (29).

$$I(\mathbf{g}) = \sum_{\mathbf{h}} \tau(\mathbf{h}+\mathbf{g},\mathbf{h})\psi(\mathbf{h}+\mathbf{g})\psi(\mathbf{h})$$

with $\psi(\mathbf{g}) = U_g \exp(i\varphi_g)$ and $\tau(\mathbf{g},\ \mathbf{h})$ the transmission function.

This has been achieved by using Stadelmann's EMS programs.

The amplitudes and phases of the (022) and (020) beams for GaAs (named g) In As (named i) and AlAs (named a) were calculated for an incident electron beam along $< 100 >$, and are presented in figure 1. It can be clearly seen that there is a noticeable difference between the GaAs and AlAs beams, while the GaAs and InAs beams show the same behavior. In figure 2 the amplitudes and phases of the $(11\bar{1})$ and (200) beams for the same compounds are drawn, and the conclusions are the same. This result does not allow the GaAs and InAs films to be distinguished from the interference processes.

The distinction between the mean intensities of the InAs or GaAs layers essentially comes from differences in the structure factor F_{hkl} depending on the gallium or indium content. F_{hkl} is proportional to the difference in atomic scattering factors f of the Group III and the Group V atoms. $(F_{hkl}\alpha(f_{\mathrm{III}} - f_{\mathrm{V}}))$. This is small for GaAs, since the difference between the scattering factors f_{Ga} and f_{As} is slight. For InAs, F_{hkl} is much greater than for GaAs, as f_{In} and f_{As} differ by about 10%. The InAs film thus appears darker than the GaAs film on a positive print.

Thus a direct analysis of high resolution images was made by measuring the scattering. In this work this was achieved by obtaining the mean value of the contrast over at least 14 $(02\bar{2})$ planes, the growth direction being [100], the zone axis during observation [011] (see Fig. 3), and the distance between two pixels corresponding to 0.02 Å.

An 0.9 ML thick InAs film, in GaAs (ML 1) was studied in this way. The high resolution image and corresponding intensity profile are shown in figure 3. *The contrast varies over five layers, instead of one.* This difference can result from several factors: 1) the lack of accuracy in this approach 2) the intrinsic phenomenon of multiple diffraction of electrons at interfaces, 3) an actual spreading of indium atoms in the structure, resulting either from a diffusion or a segregation process.

In order to evaluate the effect of the multiple diffraction at the interface, the image of a single InAs layer embedded in GaAs has been simulated (Fig. 4). The contrast was calculated for a thickness close to 30 nm. Such a large thickness was chosen since InAs is not clearly visible for thinner specimens. The contrast was also calculated for the Scherzer defocussing distance that is $\Delta f = 60$ nm, so as to obtain the bright atomic column. It was found experimentally that the

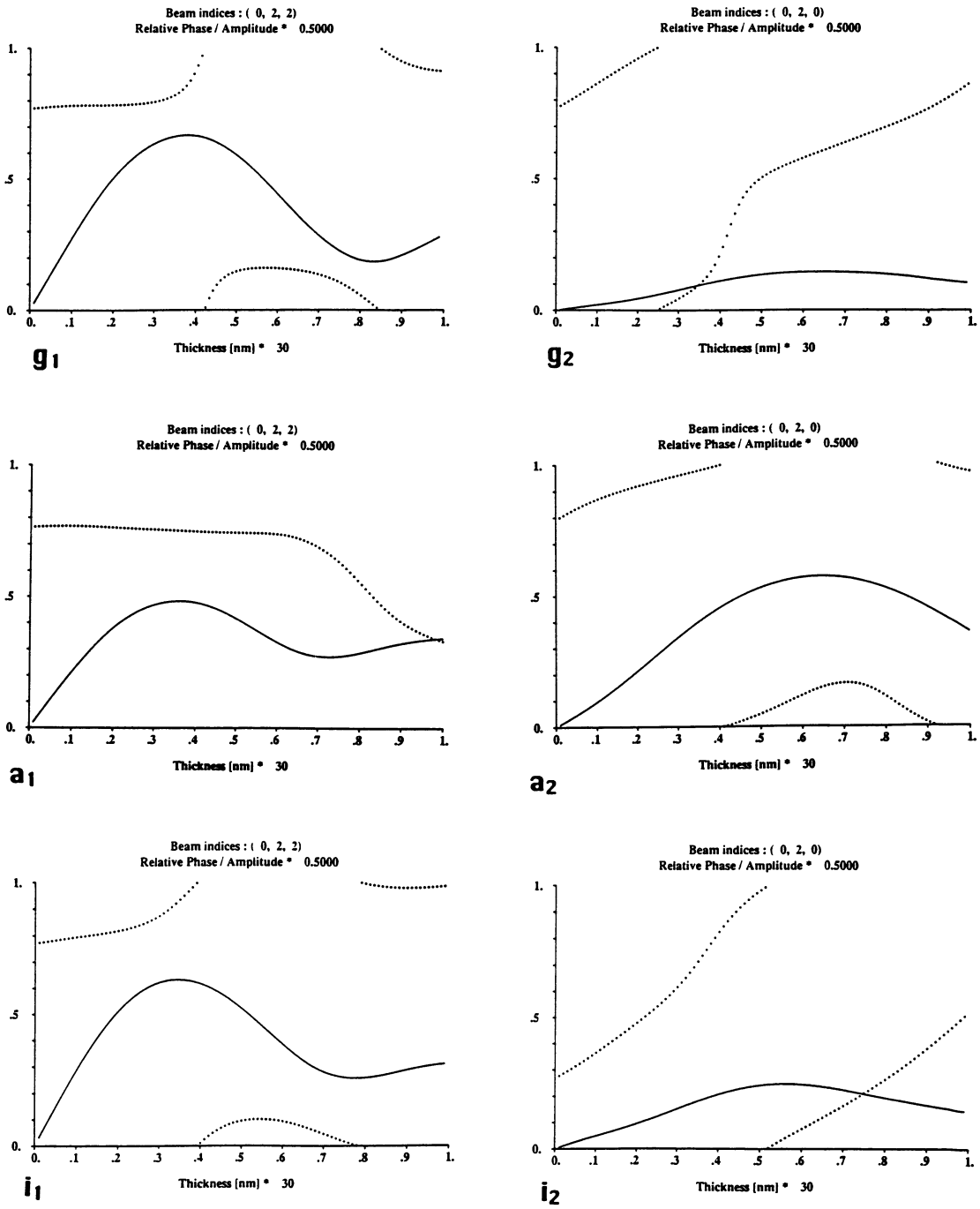

Fig. 1. — This figure shows amplitude and phase calculations for GaAs(g), InAs(i) and AlAs(a). The zone axis is [100] and the beams are the preponderant beams in this direction relative to the (000) beam, that is (022) and (020).

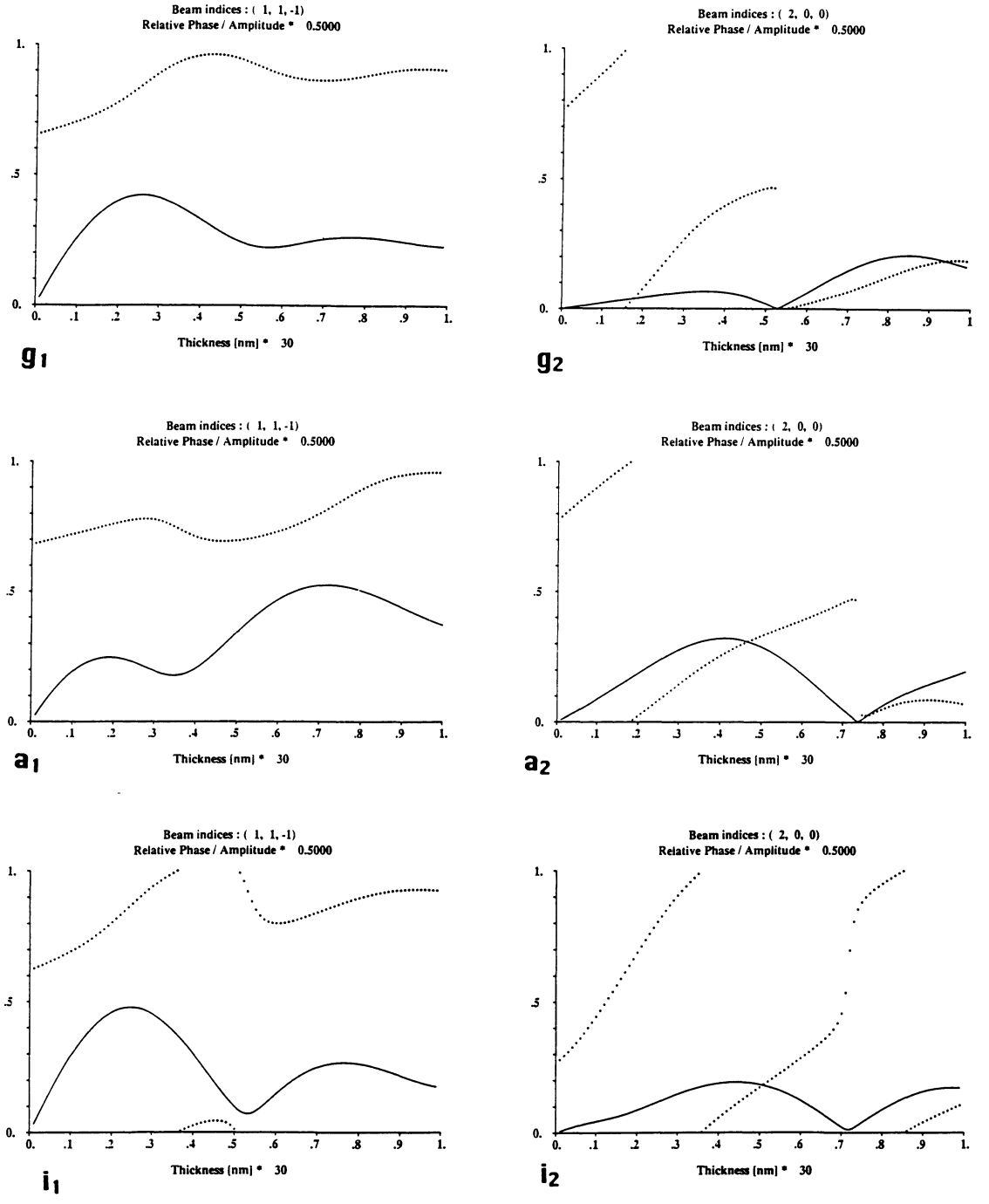

Fig. 2. — This figure shows computations of amplitude and phase for GaAs(g), InAs(i) and AlAs(a). The zone axis is [011] and the beams are the preponderant beams in this direction relative to the (000) beam, that is ($11\bar{1}$) and (200).

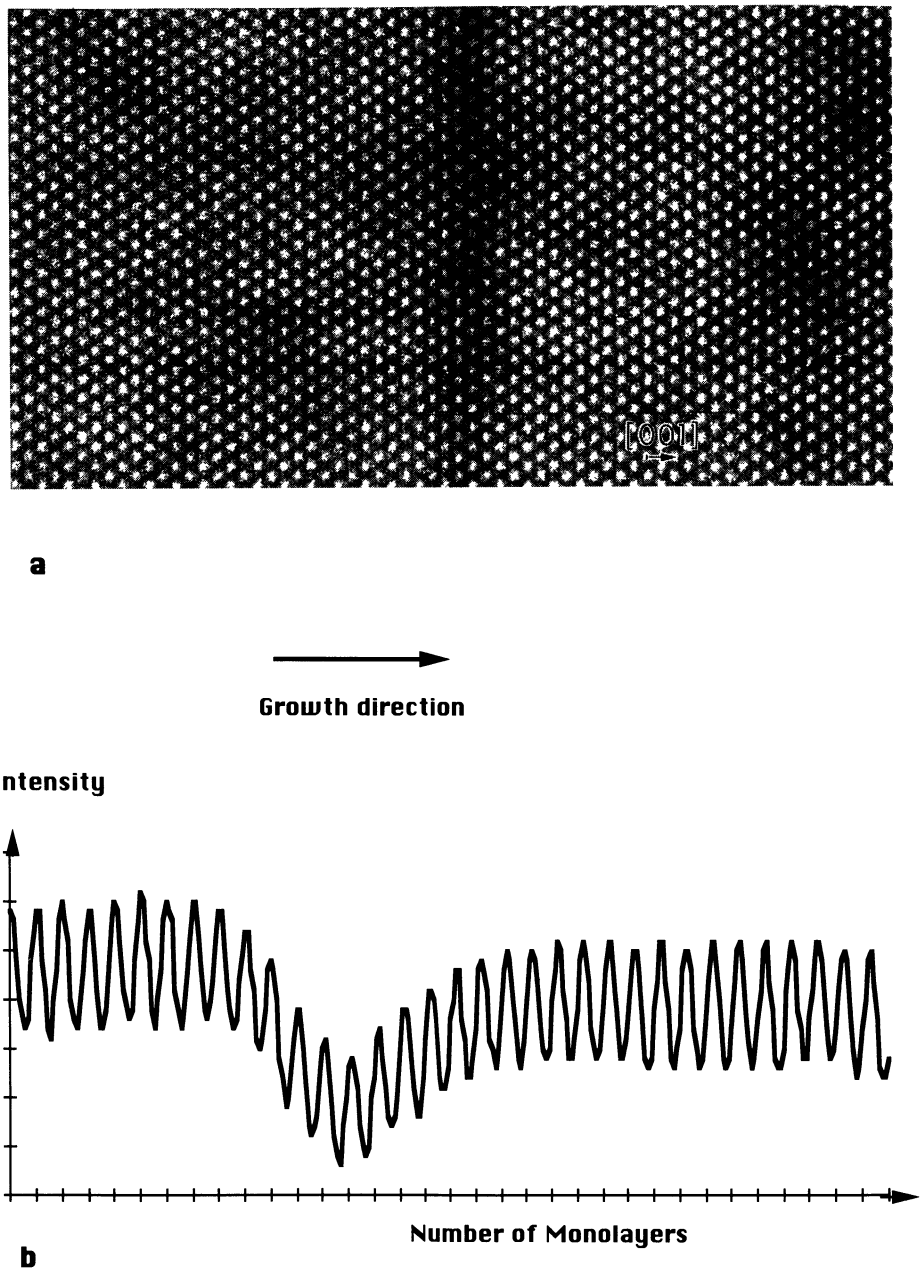

Fig. 3. — a) High resolution image of quantum well ML1, 0.9ML of InAs in GaAs, b) Profile along the growth direction < 001 > of the intensity in image (a). (The intensity is averaged in the (001) plane).

difference in contrast between InAs and GaAs was greatest for relatively thick areas and a bright column contrast. This was confirmed by calculations; indeed the image contrast when the atomic columns are dark is 1.4, whereas when they are bright it is 1.8. Thus all the images shown in this paper were obtained under the above conditions.

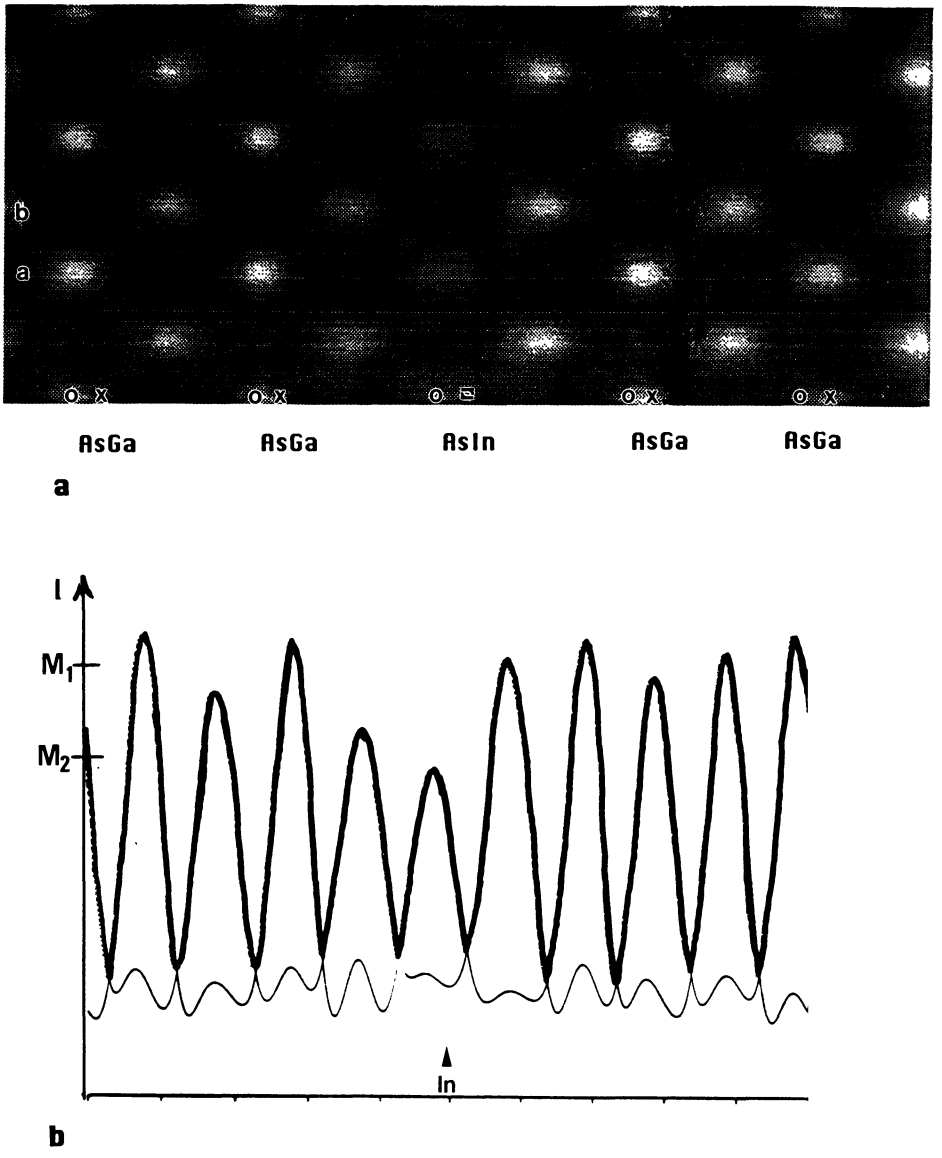

Fig. 4. — Image of one monolayer indium embedded in GaAs film simulated using EMS program. In 4a the superimposition of atomic positions (In⟺, As 0, Ga X) and the image simulated for a 30 nm thick specimen and a 60 nm defocussing distance, 4b is the intensity profile of layers a and b of the simulation (4a).

Figure 4a presents the superimposition of the simulated image and atomic positions, and figure 4b the intensity profile, where the profil of two (110) layers are superposed. The intensity M2 corresponding to the (001) InAs ML is lower than that of GaAs (M1) over two MLs instead of one, this can be explained by modification of the Ga-As interatomic distance due to the strained indium layer. The nonuniformity of the intensity in the bulk (peak height about M1) is due to computation induced boundary effects. This simulation shows that the contrast of one InAs monolayer differs

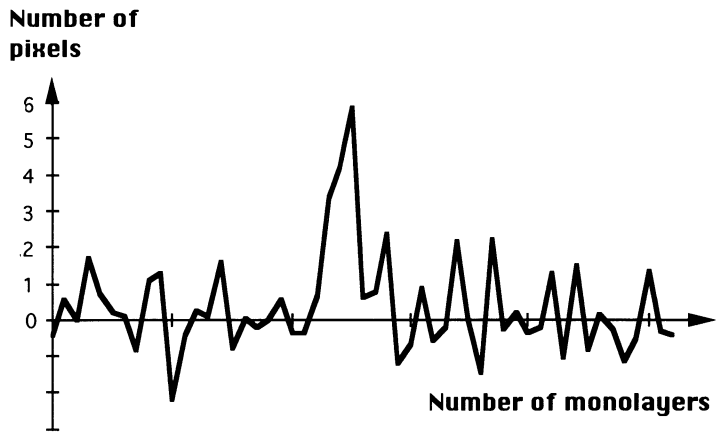

Fig. 5. — Relative displacement of atomic column projection in the image of ML1 shown in figure 3a.

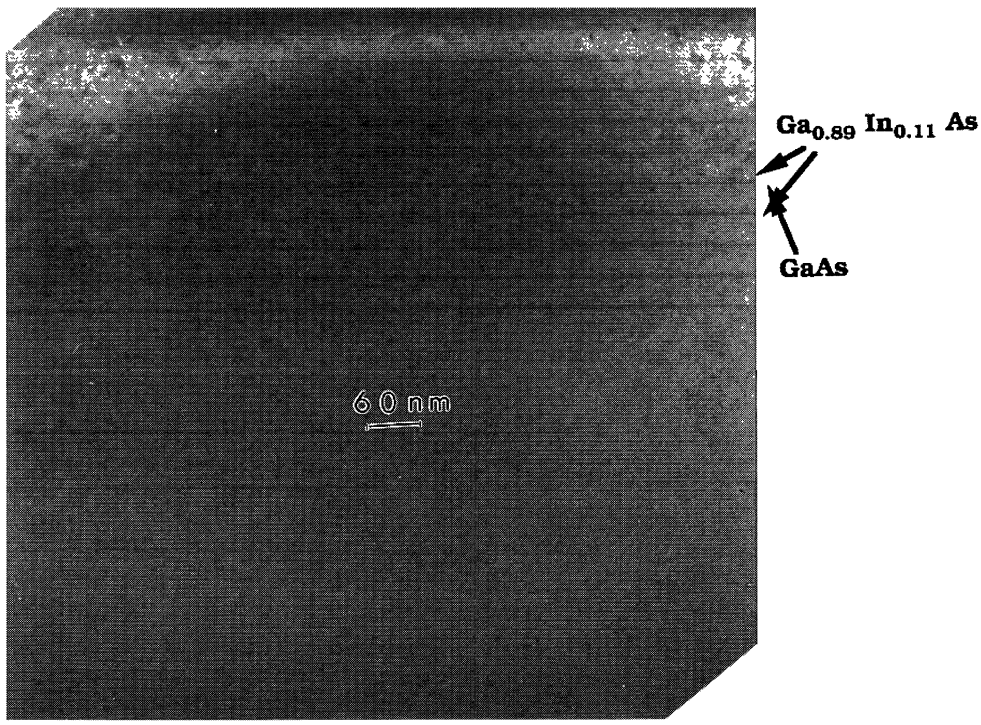

Fig. 6. — This conventional transmission electron microscopy image shows the multilayer CL1: $In_{0.11}$ $Ga_{0.89}$ As/GaAs. While containing only 11% of indium, the (InGa)As layers are very well imaged.

from that of the bulk over two monolayers.

This proves that the low intensity measured over 5 MLs for ML 1 results from a spreading of indium.

In parallel with the measurement of the mean intensity, the image can be analyzed by taking into account the strain in the film since the lattice mismatch is about 7%. There are two means

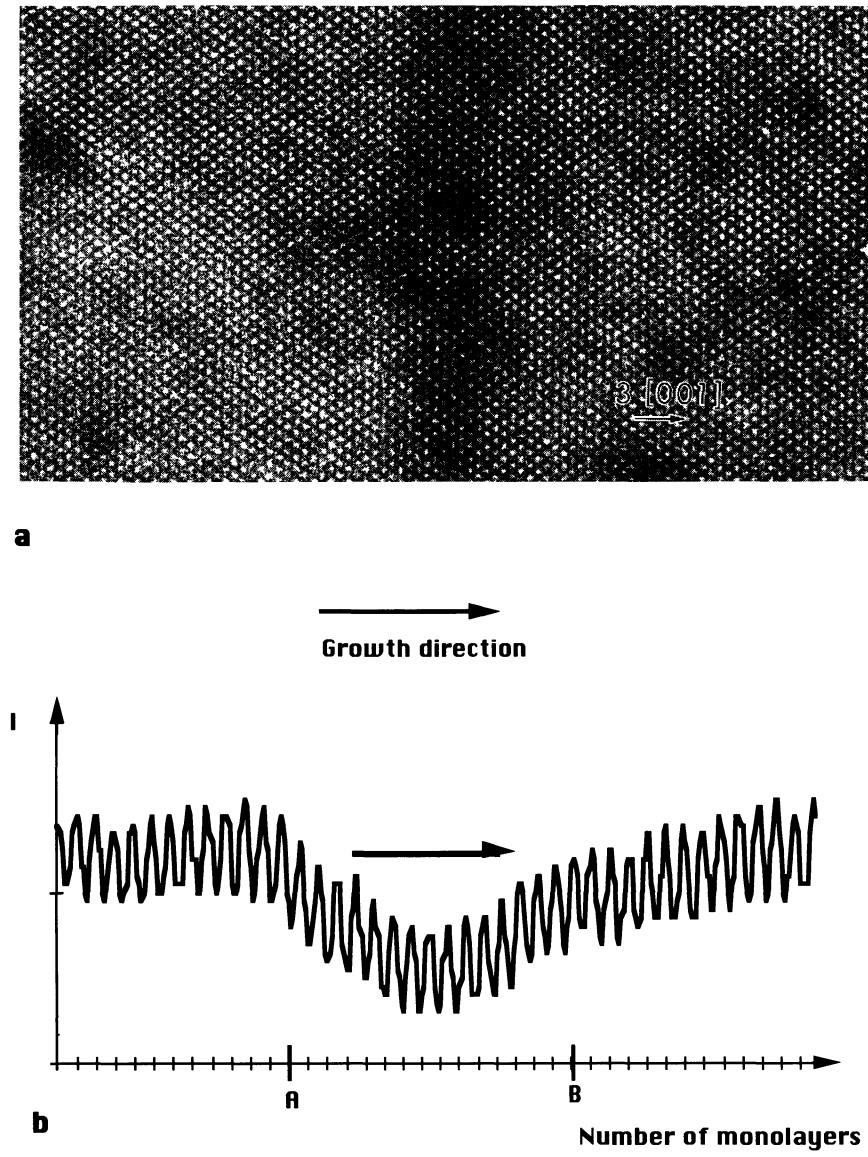

Fig. 7. — High resolution image of CL1 (7a) and the corresponding intensity profile (7b). The GaInAs/GaAs interface is less abrupt than the one in ML1.

of detecting the corresponding strain: firstly, by analyzing the strain contrast using the two beam technique, in our case it was shown that for a 4 ML. InAs film, such a contrast can be observed [3]. However, while the growth is still three dimensional for 2 ML thick films, the strain contrast is not visible because of the too small particle size. Secondly, by measuring the lattice constant directly on high resolution imaging micrographs. This has been done previously [22] directly on the image by superimposing a reference lattice onto a strained lattice. In this work the method developed by P.H. Jouneau *et al.* [25] has been used.

The result for ML1 is shown in figure 5. We measured a detectable distortion over 3 ML instead

of 5 obtained by the mean intensity measurement (Fig. 3). The maximum distortion is 6 pixels, that is 0.015 nm which corresponds to a 2.3% mismatch, and thus not to a pure InAs layer.

For such a measurement, the experimental conditions must be verified very precisely: a misalignment of the microscope induces a shift in atomic projection and this shift depends on **g** (the diffracted beam wave vector). As **g** is different for GaAs and InAs, an error can be made. One way of being sure about the alignment is to verify the measurement over a range of defocussing distances, as the error is a function of Δf. Moreover, if there is a tilt of the sample, the shift will be the same for InAs and GaAs and would thus not induce an error in the distortion measurement. The measured distortion should be discussed from two points of view.

Does the strain of the InAs layer have any influence on the GaAs substrate? Do the polished surfaces have any influence on the InAs relaxation? Concerning the second point we mentioned earlier that it is necessary to work in thick GaAs areas (about 30 nm) to detect a good contrast difference between GaAs and InAs. For this value it has been shown that the surface has no influence [30]. It is difficult to solve the first point with this experiment as the interface roughness is over one monolayer, and can therefore modify the InAs structure [31]. In any case, when comparing with the mean intensity measurements (Fig. 3b), one can observe that the distortion measurement is less sensitive to a low indium concentration film, but corresponds to a GaInAs film.

Subsequently the sensitivity limits of the two means of image analysis described above were compared by studying a 10 ML $Ga_{0.89}$ $In_{0.11}$ As/GaAs multilayer (CL1). A low magnification view of this structure (Fig. 6) shows that the layers are clearly visible. The intensity in the high resolution images was measured and is shown in figure 7. Considering that the mean value of the minimum is not the same below and above the GaInAs layer (which may be due to a variation in the thickness of the specimen), the extension of the indium covers 16 layers between A and B in the figure. This result shows that less than 11% of indium can be detected using the scattering contrast. On the other hand, using the lattice constant measurement technique, the distortion measured is zero. The distortion must be too small and not abrupt enough because the measurement is performed by differentiation.

In this part we have demonstrated that indium is best detected by measuring the scattering contrast on high resolution images and that an *indium concentration as low as 6% can be detected.*

4. Analysis of the experimental results.

4.1 InAs ON GaAs - 2D OR 3D GROWTH? — The MBE growth is monitored by RHEED. This technique tends to prove that the transition between two dimensional (2D) and three dimensional (3D) growth occurs for a 1.7 InAs monolayer (ML). Thus we compared 0.9 ML (ML1) and 1.7 ML InAs films (ML2) (Fig. 8). On the high resolution image, the InAs/GaAs interface appears to be quite abrupt while the roughness is significant on the GaAs/InAs interface. This is confirmed by the intensity profile in figure 8. The average intensity decreases over two layers, is minimum over three layers, and then recovers over 5 layers. The decrease over two monolayers confirms the simulation shown in figure 4. If we compare the evolution of ML1 with that of ML2, it can be seen that they are quite similar.

This result shows that the evolution from the two dimensional growth to the three dimensional growth is not linked to a clear structure variation. Indeed the roughness of a 0.9 ML thick InAs film analyzed on HREM images is significant. This roughness could not be observed by RHEED *in-situ* control or by using the two-beam TEM technique. In the RHEED experiment the contrast is proportional to the island size. We thus suggest that either the island size of ML 1 is too small to be detected, and the surface thus seems to be uniform using the RHEED technique, or that there

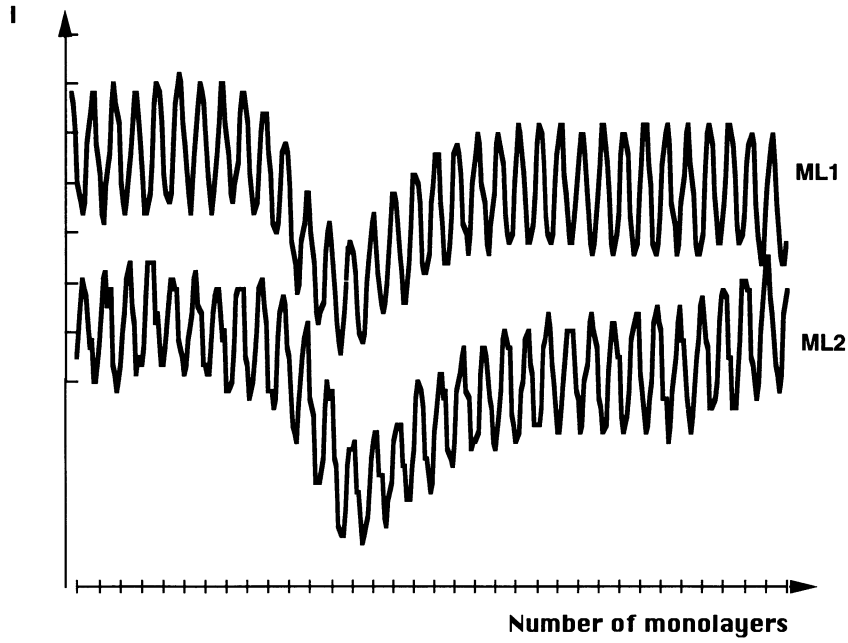

Fig. 8. — This figure compares the intensity profiles for ML1 and ML2. The InAs/GaAs interface shows the same abruptness, the GaAs/InAs appears less abrupt.

really is a 2D growth of a 1 ML InAs film. However, as the covered monolayer is analyzed using HREM, we can detect the degradation of the flatness due to GaAs overgrowth. As quantum well structures require this GaAs cover, one should not be too confident in the RHEED results. These results show that the high resolution electron microscopy technique allows more direct confirmation of roughness than X-Ray standing waves [34]. Can we obtain short period superlattices in these conditions?

4.2 COMPARISON OF TWO GROWTH MODES FOR STRAINED InAs/GaAs SHORT PERIOD SUPERLATTICES (sps). — The growth by MBE of $(InAs)_n(GaAs)_m$ on InP has been reported for sometime [12, 13]. Such layers however display rather poor structural and optical properties, as a result of a degraded growth mode. A shift from 2D to 3D growth mode is revealed by a bulk type spotty pattern when about 5 MLs of InAs or GaAs have been deposited by MBE on a buffer layer lattice-matched to InP under standard growth conditions (500 °C, As-stabilized surface). During the growth of a $(InAs)_n(GaAs)_n$ SPS, for n smaller than the apparent critical thickness for 3D growth of the individual layers ($2 \leq n < 5$), a continuous shift to 3D growth can be observed by RHEED. Some intensity modulation of the integral order streaks gradually appears and a bulk-type spotty pattern is finally obtained, when typically 50 nm ($n = 4$) or 90 nm ($n = 3$) thick layers have been deposited. This degraded growth mode is responsible for the poor structural and optical quality of MBE grown SPS.

A clear improvement in the overall growth process results from an alternate delivery of arsenic and metal atoms by monolayer increments at low temperature (350 °C) [17]. This modulated MBE (MMBE) allows bidimensional InAs and GaAs layers to be deposited on InP up to the critical thickness for plastic relaxation (and obviously beyond). No degradation of the growth mode can be observed for $(InAs)_n(GaAs)_n (n \leq 8)$ for 100 nm thick films. The alternate deposition

of As4 and metal atoms forces a layer by layer growth mode of the highly strained layers, thus allowing the growth of high quality material. (However, this forced 2D growth mode can only be observed for temperatures lower than about 400 °C).

Since SPS layers grown by standard MBE undergo a continuous degradation, it is important to test the structural and optical qualities of the SPS at the first stages of its formation. For this purpose, we have grown and studied several multiquantum well structures using (InGaAl) As barriers, and a 10.5 nm thick $(InAs)_2(GaAs)_2$ SPS as "well" material. The buffer and barrier layers were grown by MBE at 520 °C, whereas the SPS layers were either deposited by standard MBE (CL2a) or MMBE at 350 °C (CL2b). The Photoluminescence (PL) and PL excitation spectra obtained at 2 K for both samples are shown in figure 9a. The excitation spectrum is smooth for CL2a (Fig. 9-2). Which indicates that the MQW structure has no bidimensional behavior. Contrasted areas on the high resolution transmission micrograph obtained for CL2a (Fig. 9-4) reveal the in-plane inhomogeneities within the well material. These contrasts correspond to strain localized at the interface. The 2D features of the MQW excitation spectrum are reduced if the bandgap variations they entail are of the order of the spacing between the optical transitions. For a 10.5 nm thick quantum well, this effect reveals in-plane fluctuations of the average composition of the SPS exceeding 5%. On the other hand, the observation of bi-dimensional step-like features and the recovery of excitonic peaks in the excitation spectrum for CL2 b (Fig. 9-1) confirm a remarkable improvement for the MMBE grown $(InAs)_2(GaAs)_2$ SPS. Its homogeneity is also revealed by the high resolution micrograph displayed in figure 9-3, on which alternate bilayers can clearly be identified. The intensity measurement of the HREM image (Fig. 10) shows that a periodicity, pointed X, is maintained.

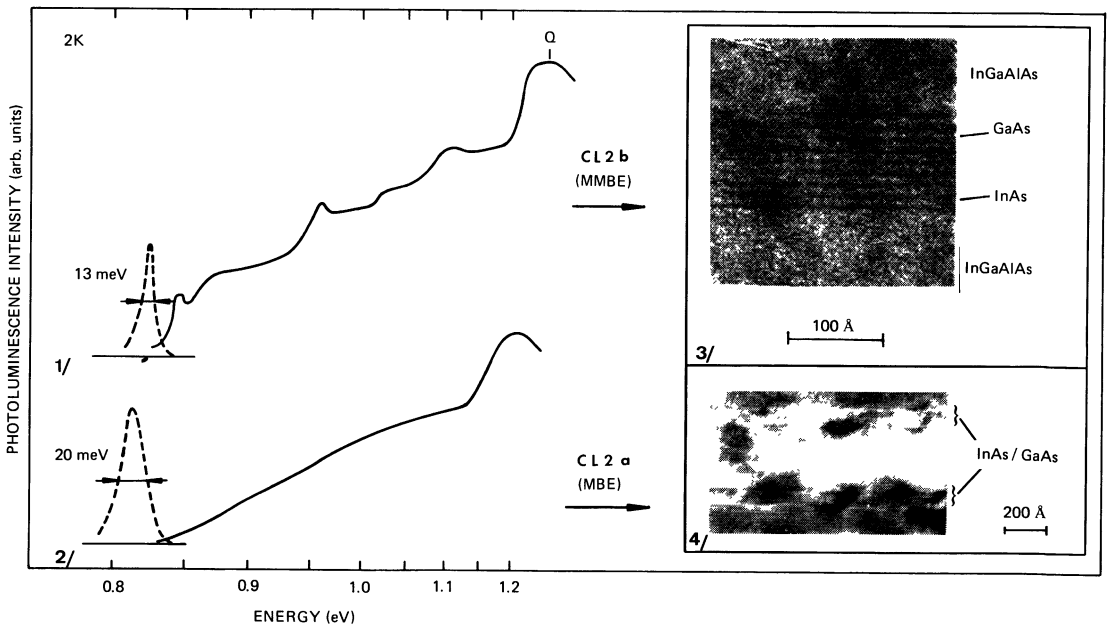

Fig. 9. — Photoluminescence spectra obtained from standard MBE (CL2a) and (CL2b) growth quantum wells (2 and 1). And their respective TEM images (4 and 3).

The drastic degradation in the growth mode in MBE (CL2a) result from the influence of existing inhomogeneities on the growth mechanism, via the strain field they generate. Let us consider for instance and indium rich region of the SPS, close to the SPS surface. The surface tends to adopt a larger in-plane parameter above this defect; as a result, the growth of InAs is favored (and the growth of GaAs partially inhibited) in this region, which leads to an overall increase in the in-plane inhomogeneity during growth. (Similarly, this effect can lead to a correlation of the position of the defects, as shown for some InAs/GaAs multiquantum well structures grown on GaAs [3]).

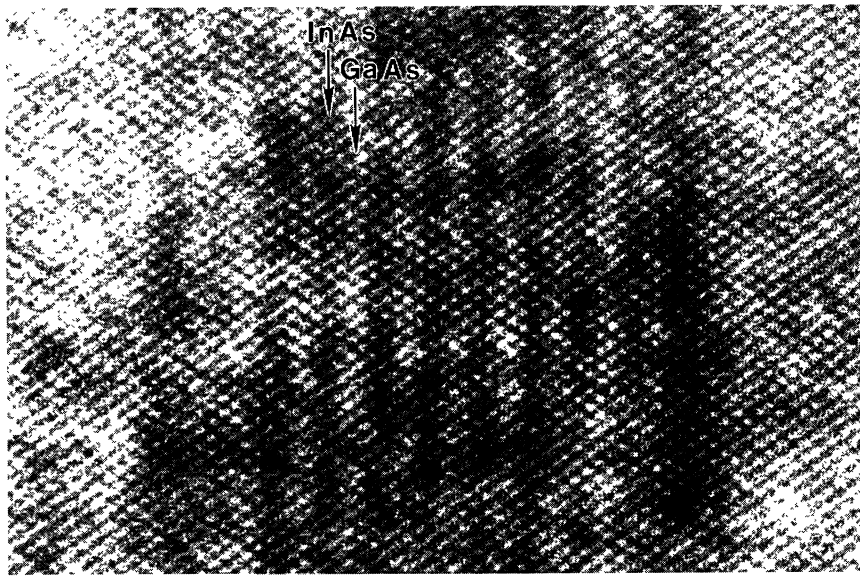

a

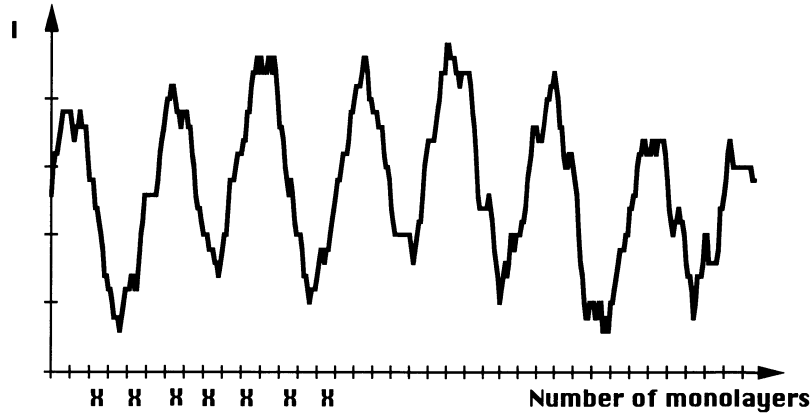

b

Fig. 10. — Intensity profile (b) of high resolution image (a) along the growth direction of an 8 period $(InAs)_2/(GaAs)_2$ short period superlattice (CL2b); in b the half periodicity is pointed X.

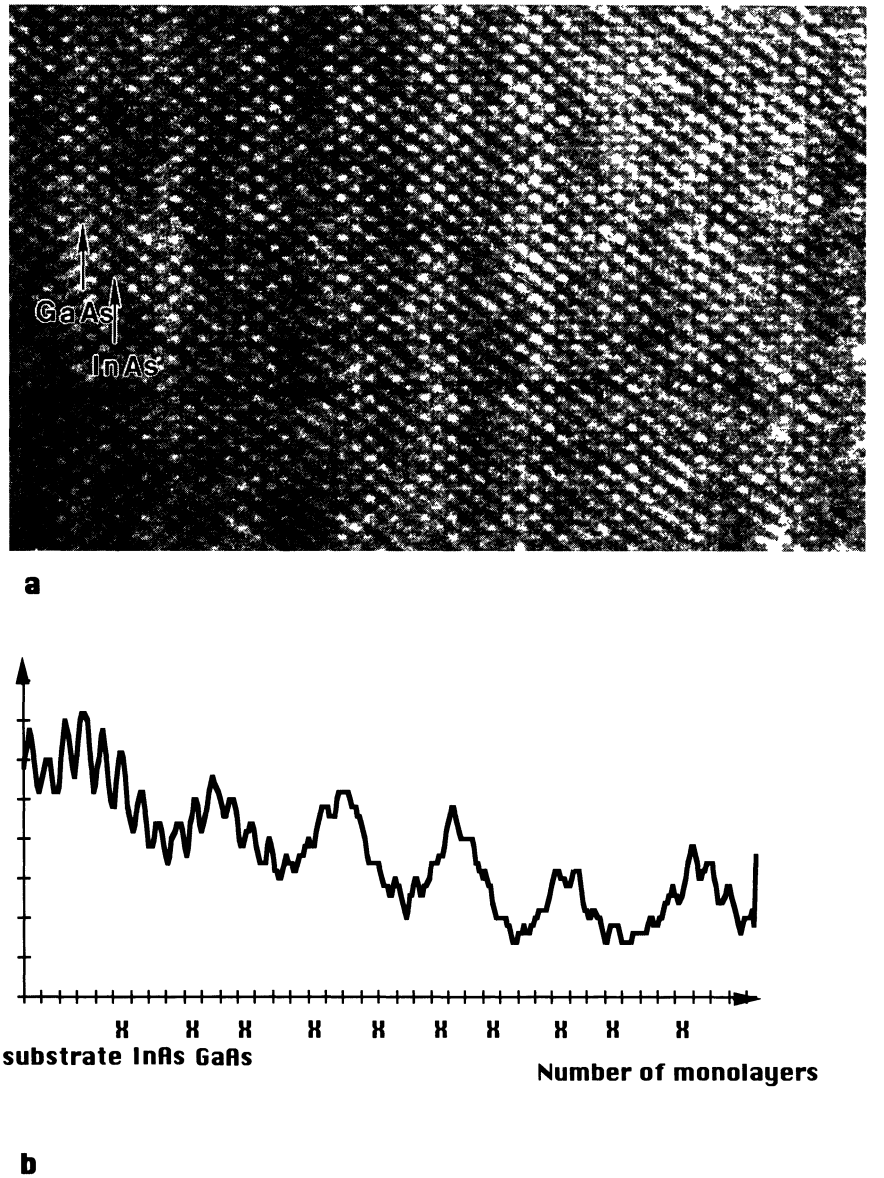

Fig. 11. — The $(InAs)_3/(GaAs)_3$ multilayer (CL3). The high resolution image (a) allows a mean intensity value of the layers (b) to be obtained; in b the expected interfaces are pointed X.

MMBE overcomes this intrinsic tendency of highly strained layers to grow three-dimensionally, as shown not only for InAs/GaAs, but also for other III-V highly strained systems such as InAs/AlAs and GaAs/GaP [2] (The detailed mechanism by which MMBE forces a layer by layer growth mode has been described elsewhere, and will not be discussed here [17]). As a result, much thicker SPS layers can be grown without any apparent degradation of the growth process. For instance, the high resolution micrograph shown in figure 11a has been obtained on a 100 nm thick $(InAs)_4(GaAs)_3$ SPS. The intensity profile shows (Fig. 11b) that the periodicity measured is close

to InAs4 - GaAs3. This corresponds to X-Ray or Raman measurements.

This experiment proves that the *MMBE growth allows thick superlattices of InAsGaAs 4 ML thick films to be obtained* keeping a well defined periodicity.

However, the contrast is smooth showing that there is still a mixing of indium and gallium atoms as demonstrated below.

4.3 EVIDENCE OF SURFACE SEGREGATION OF INDIUM ATOMS IN InGaAs BASED HETEROSTRUCTURES. — As shown previously, indium atoms are spread over 5 MLs, typically in the final structure when 1 ML of InAs is nominally inserted into the GaAs matrix. The asymmetric In composition profile suggests that thin broadening of the indium containing layer comes from a surface segregation of In atoms rather than from a diffusion process. In order to confirm this result, we studied in detail the absolute displacement of the indium atoms with respect to their nominal position. For this purpose, the InAs ML was inserted in a GaAs/AlAs quantum well. The GaAs/AlAs interfaces are very abrupt on the ML scale since they are only weakly affected by segregation processes. As a result, they can be used as markers when studying the location of In atoms. Two symmetrical stuctures CL4 and CL5 were grown at 530 °C [22]. Each multiquantum well contains three InAs/GaAs/AlAs asymmetric quantum wells, for which the 1 ML thick InAs layer is nominally inserted at a given distance n from the (first grown) GaAs/AlAs interface in CL4 (this AlAs layer is named bottom) or from the AlAs/GaAs interface in CL5 (this AlAs layer is named top), where n is equal to 3, 5 or 7 MLs for the three quantum wells respectively, and the well width is in all cases 28 MLs. AlAs barriers are nominally 3MLs thick, and the quantum wells are embedded in thick $Ga_{0.7}$ $Al_{0.3}$ As layers. Low resolution micrographs obtained for these structures are shown in figure 12.

Figure 13 corresponds to the quantum well width $n = 5$ of sample CL4. The intensity measured on the micrograph shown in figure 13a is the highest for the 3 AlAs MLs (Fig. 13b). This is followed by a first decrease in intensity corresponding to the five GaAs MLs. Then the intensity decreases more sharply over five MLs to recover its initial value about eight MLs further on. This result shows that there is a high indium concentration over three MLs and then a slow decrease over a wide extent.

Figure 14 corresponds to sample CL5. The three quantum wells having respectively $n = 3$, 5 and 7 were studied. The quantum wells having $n = 3$ MLs were analyzed using both the lattice constant and contrast measurement. The indium level can be detected either by a decrease in intensity (Fig. 14b) measured on the micrograph (Fig. 14a) or an increase in lattice constant (Fig. 14c). It is clear (Fig. 14b) that the contrast associated with GaAs is not recovered before the AlAs film; that is indium atoms spread throughout this layer during growth. The lattice constant measurement (Fig. 14c) offers a supplementary result: the AlAs parameter is lower than that of the GaAs, and this is the case for the three quantum wells ($n = 3$, 5 or 7). This cannot be understood using the uniform planar strain model, but could be interpreted taking into consideration the interface steps [22].

This experiment clearly confirms that *this asymmetric redistribution of indium atoms is due to a segregation process*, and not to a bulk diffusion process at growth temperature (which would also lead to a spreading of indium atoms into the layer below the nominal InAs layers).

It is particularly interesting to study the location of the first ML containing indium. Equilibrium models of the segregation process [15] assume the existence of an exchange reaction on a microscopic scale between In and Ga atoms; when an extra ML (s) is deposited during growth, an exchange reaction occurs between this new surface ML and the previous one ($s - 1$). Since the bond energy is smaller for In-As than for Ga-As bonds, the presence of In atoms at the surface is favorable, the surface ML (s) is always more rich in indium than the first buried ML ($s - 1$) and the In composition get the x_{eq} value (Fig. 15a). However, due to the entropy term in the ex-

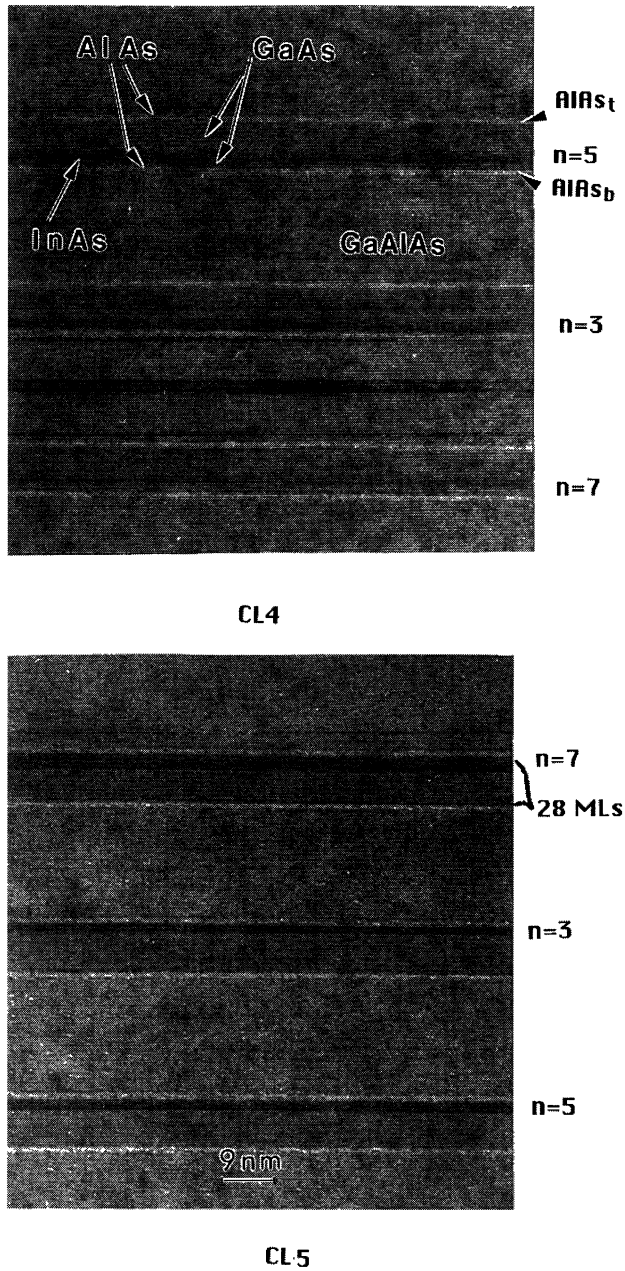

Fig. 12. — Low magnification image of CL4 and CL5 InAs/GaAs/AlAs QW structures, nominally symmetrical with each other.

pression of the free energy, the indium atoms of this surface bilayer are not all segregated in the surface ML. A part of these indium atoms is incorporated in ML $s - 1$. When GaAs is deposited on InAs, this partial surface segregation and progressive incorporation of the indium atoms leads to the typical composition profile shown in figure 15b.

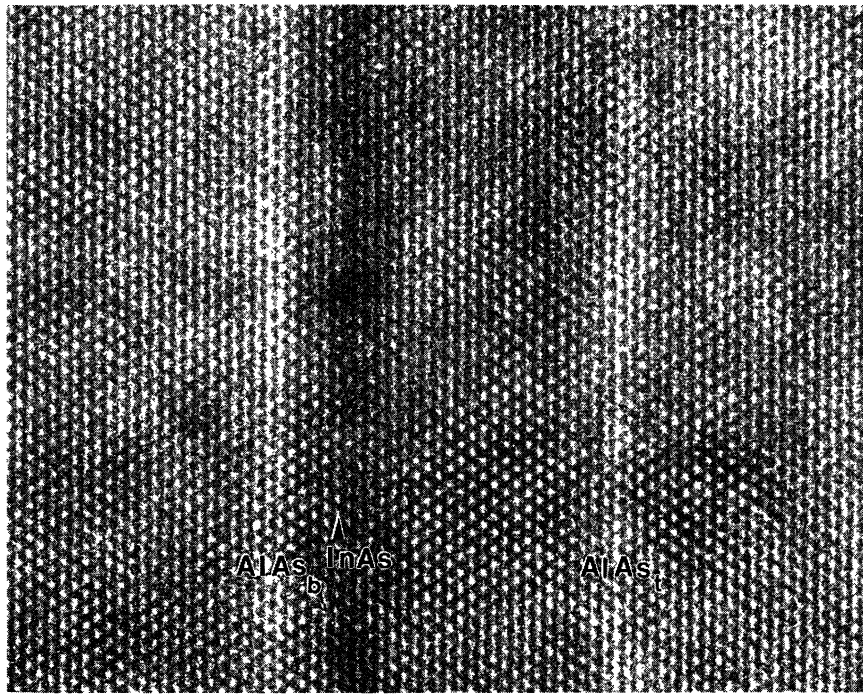

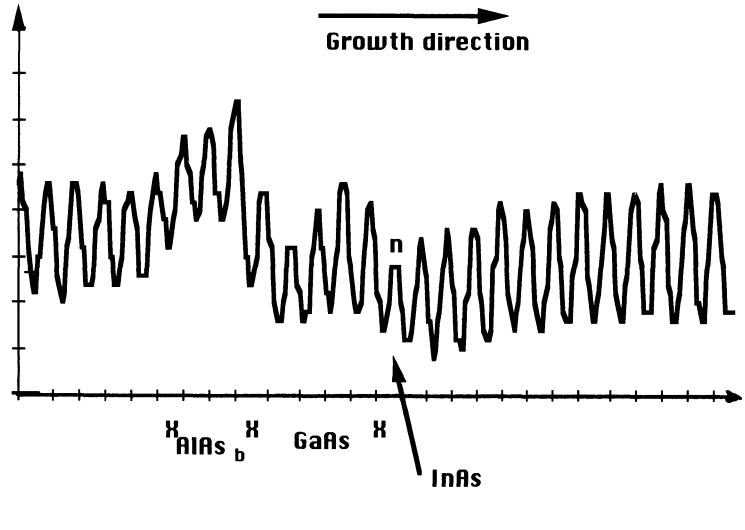

Fig. 13. — High resolution image and intensity profile for sample CL4. Here, 5 MLs of GaAs were deposited between the $AlAs_b$ bottom layer and the InAs ML; X corresponds to the determined interfaces.

When 1 ML of InAs is deposited on GaAs, an exchange reaction should occur, in order to increase the entropy of the surface, and lower the overall free energy of the film. As a result, equilibrium models predict an incorporation of In atoms in ML $(n - 1)$, and upper MLs, if the

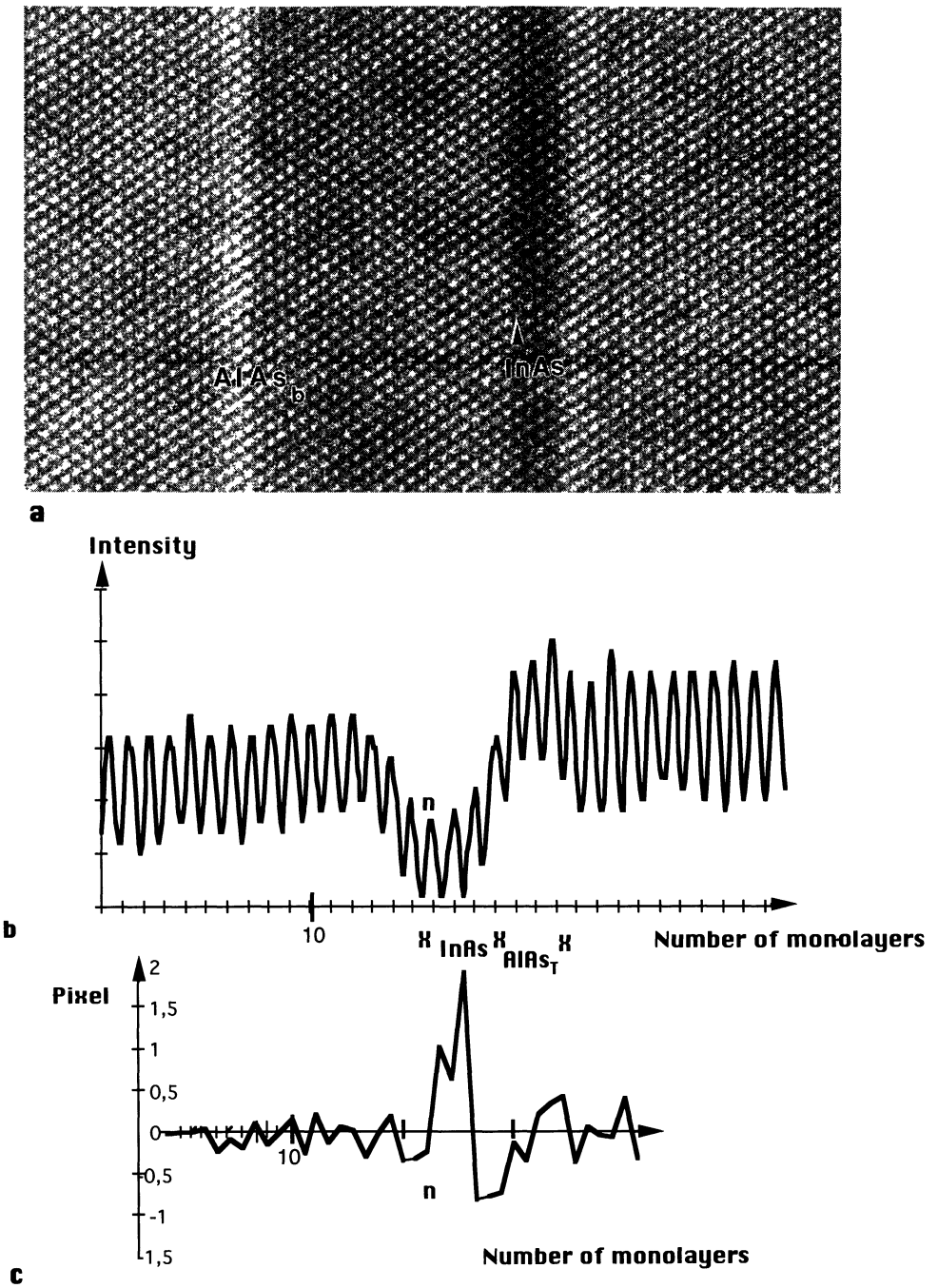

Fig. 14. — High resolution image of sample CL5. Here, 3 MLs of GaAs were grown (a). The intensity profile of the layers (b) and lattice displacement (c) measurements are compared; n is the position of the first In deposited layer, X the determined interface.

nominal position of the InAs ML is n. Futhermore, the maximal indium composition in the final structure is predicted in this frame to be reached for ML $(n-1)$.

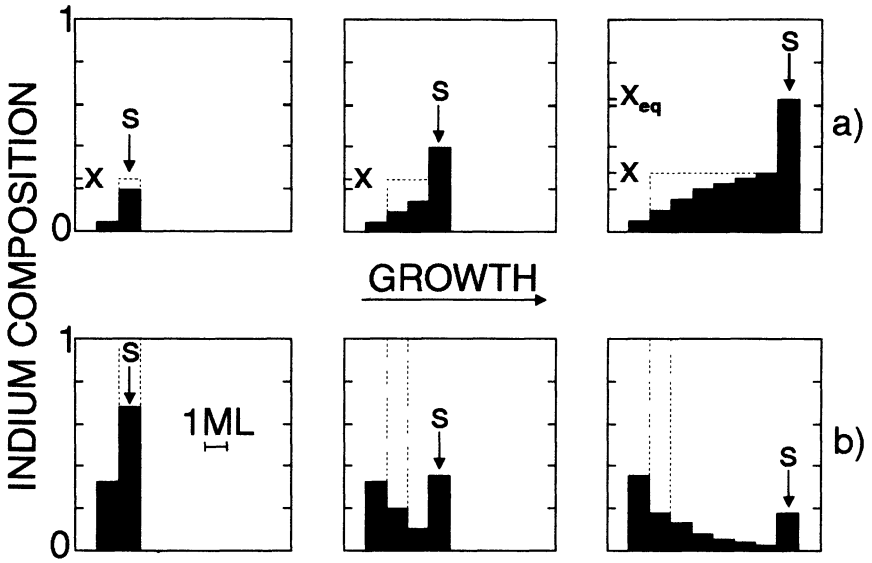

Fig. 15. — Calculated composition profile for "InGaAs on GaAs" (a) and "GaAs on InAs" (b) interfaces in the equilibrium segregation model, for various thicknesses of the overlayer. "s" designs the position of the surface ML. The nominal indium composition (x) profile is indicated in each figure by a broken line (x_{eq} is the equilibrium composition).

If we now consider figures 13b and 14b, we can see that the brightness of ML $(n-1)$ is always very close to that observed for pure GaAs and corresponds to the calculation shown in figure 4; on the other hand, the first ML containing a large amount of indium is apparently ML n. This experiment reveals very clearly that the exchange reaction does not occur (or is very far from reaching the equilibrium configuration of the surface) when InAs is deposited on GaAs.

Samples CL4 and CL5 were also studied by low temperature (8 K) photoluminescence. Bandgap differences as large as 30 meV were observed for such pairs of InAs/GaAs/AlAs asymmetric quantum wells nominally identical but for the growth direction. This bandgap difference is obviously due to the surface segregation of indium atoms. On average, these atoms drift towards the top GaAs/AlAs interface in sample CL5, and towards the centre of the GaAs/AlAs quantum well for sample CL4. The electronic gap of the QW is therefore respectively enhanced (for CL5) and reduced (for CL4) with respect to its nominal value. This experiment highlights how deeply segregation processes can affect the electronic properties of such QWs. This high sensitivity of the bandgap difference for pairs of asymmetric InAs/GaAs/AlAs samples (identical but for the growth direction) allows the segregation process to be studied in detail. A comparison of these experimental results with theoretical estimates (obtained for various composition profiles for the indium containing layer) has been undertaken [18]. To account for the experimental data the composition of ML $(n-1)$ must not exceed 0.05, and the best agreement can be observed when we consider that *no exchange reaction occurs when InAs is deposited on top of GaAs, in agreement with HREM data. In contrast, no deviation can be observed from an ideal equilibrium segregation scheme for the GaAs on InAs interface* in this optical experiment; a precise estimate of the segregation amplitude has been obtained, which confirms and refines previous measurements obtained by surface analysis techniques. This breakdown of the equilibrium segregation model for the InAs on GaAs interface alone is worth clarifying. We have attributed this important effect ot a kinetic freezing

of the In/Ga exchange reaction. This reaction would indeed require the breaking of very stable Ga-As bonds, when InAs is deposited on GaAs, for surface Ga atoms to be exchanged with incoming indium atoms. On the other hand, when a GaAs ML is grown on top of an indium rich layer, the In-As bonds are broken for exchange reactions to occur. Since In-As bonds are much weaker than Ga-As bonds, it is clear that, at the growth temperature, a kinetic freezing of the exchange process is likely to occur for the InAs on the GaAs interface alone.

This experiment proves that the *indium exchange is due to out of equilibrium segregation* into GaAs upper layers and not to diffusion.

4.4 NEW METHOD FOR THE GROWTH OF InGaAs/GaAs QUANTUM WELLS WITH ABRUPT INTERFACES. — As shown previously, the progressive incorporation of the segregated indium atoms results in the gradual composition of "GaAs on InGaAs" interfaces. During the first stages of the growth of $In_xGa_{1-x}As$ on GaAs on the other hand, an increase in the indium composition of the surface ML can be observed experimentally [19, 20]. This enrichment due to surface segregation stops when the composition of the surface ML reaches the x_{eq} value, for which the surface ML is in equilibrium (as far as the In/Ga exchange reaction is concerned) with a bulk layer of composition x. Of course, this enrichment of the surface occurs at the expense of a reduction in the composition of the buried InGaAs layer with respect to its nominal value x. In order to eliminate the composition gradings resulting from indium segregation, we have recently proposed an original approach [20]: the composition x_{eq} of the surface ML of a thick $In_xGa_{1-x}As$ layer is measured in a preliminary experiment. A 1ML thick prelayer of $In_{x_{eq}}\ Ga_{1-x_{eq}}\ As$ is then deposited before $In_xGa_{1-x}As$ is grown. Since the surface conposition is already x_{eq}, it remains constant throughout the deposition of $In_xGa_{1-x}As$; as a result, the composition of the buried layer can (in principle) be ideally close to x. In order to avoid any incorporation of indium in the top GaAs layer, a slight thermal annealing is performed during a growth interruption. Since the desorption temperature is much smaller for InAs (540 °C) than for GaAs, it is possible to desorb selectively the indium atoms present in the surface ML. (A desorption of indium atoms from buried MLs would require bulk diffusion processes, which are completely improbable at 540 °C). Obviously, no incorporation of indium in the top GaAs layer can occur unless this desorption of the surface indium atoms is completed.

Several approaches have been adopted in order to test this technique. A detailed study of the composition of the surface ML has shown that the surface composition actually remains constant throughout the growth of InGaAs when the prelayer is used, and has been used to monitor the full desorption of the surface indium atoms at the second interface [20]. In order to validate this approach, and *ex situ* comparison of InGaAs quantum wells grown under standard conditions or using this technique was however necessary. Multi quantum well samples CL1 (standard MBE) and CL6 (prelayer+thermal annealing) were studied for this purpose. Both structures contain nominally eight (10 ML $In_{0.11}Ga_{0.89}As$)/GaAs quantum wells. High resolution X-ray diffraction was used to characterize these samples. This experiment confirmed that the total InAs quantity per quantum well (which defines the mean lattice parameter of the superlattice along the growth direction) is the same within the experimental resolution for both samples. Therefore, the different behavior of CL1 and CL6 can only result from a different distribution of indium atoms within the structure.

The high-resolution micrograph obtained for sample CL6, and the corresponding brightness profile, are shown in figure 16. A comparison with figure 7 (obtained for CL1) highlights the drastic improvement in the interfacial abruptness obtained for sample CL6. The intensity is significantly smaller than for pure GaAs only in a 10 ML thick region, as expected for a perfect localization of indium atoms at their nominal position. The intensity is essentially constant for the central MLs of the InGaAs film, and increases at the edges of the quantum well over a two

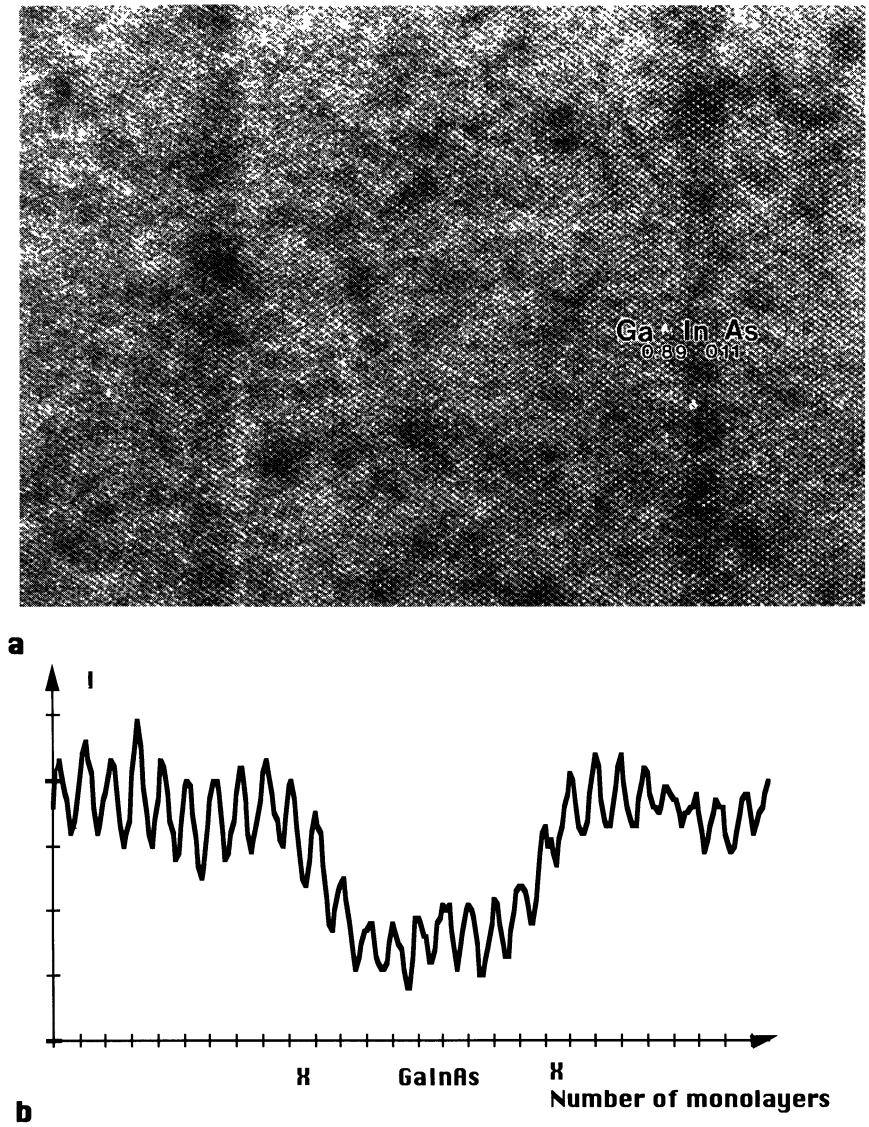

Fig. 16. — High resolution image of CL6 (16a) and the corresponding intensity profile around the $Ga_{0.89}$ $In_{0.11}$ As film. The abruptness of the composition profile is clearly shown for both interfaces of the quantum well; X is the determined interface.

ML thick region, which corresponds to our experimental resolution on composition gradients. As a result no deviation from an ideally abrupt composition profile can be observed here by HREM for sample CL6.

Figure 17 presents the low temperature PL spectra obtained for samples CL1 and CL6. Though both samples contain the same quantity of InAs per quantum well, a clear shift towards lower energies can be observed for sample CL6 with respect to sample CL1. This effect confirms a better localization of indium atoms for sample CL6 (for a given quantity of InAs, the QW has a given intergrated attractive potential for the electrons (or the holes); a better localization of this potential

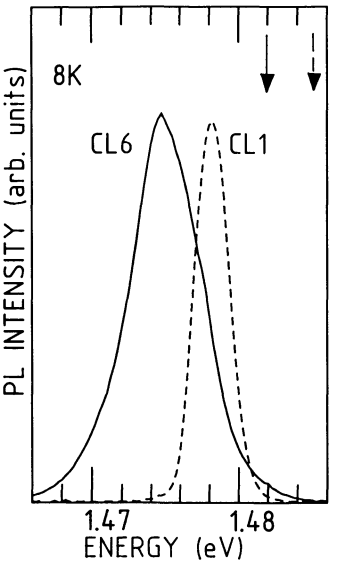

Fig. 17. — Photoluminescence spectra obtained on quantum wells CL1 and CL6. Arrows indicate their calculated bandgaps (broken line for CL1).

entails a larger binding energy for electrons and holes, and a smaller bandgap for the QW). The bandgap transition energies of both QWs have been calculated in the effective mass approximation, and are indicated by arrows in the figure. A perfectly abrupt composition profile is assumed for CL6, whereas for CL1 the composition profile predicted in the equilibrium segregation model is used. In both cases the exciton binding energy (typically 7 meV) is not included. We can see that the calculated transition energies are in good agrement with our experimental results, thus confirming that abrupt interfaces have been achieved for sample CL6.

This experiment shows that the indium segregation can be compensated by a predeposition of indium film before the growth of a ternary GaInAs over GaAs heterostructure.

5. Conclusion.

This work has demonstrated the difficulty of growing a very abrupt InAs/GaAs interface as an 0.9 ML thick film extends over about 5 MLs.

The best means of analyzing the electron images of such films has been shown, the indium segregation during growth has been proved and a new method for avoiding indium segregation in InGaAs/GaAs superlattices has been developed.

Concerning the detailed image analyzis using image simulation, distortion measurements and intensity measurements have shown that intensity measurement is the most sensitive way to detect InAs containing layers in a GaAs matrix. It is demonstrated that less that 6% of indium can be detected. HREM simulations of an InAs monolayer embedded in GaAs have shown that the layer contrast extends over two monolayers.

Moreover, concerning the superlattice growth, by combining photoluminescence measurements and electron microscopy, we have shown that the spreading of indium atoms with respect to their nominal location results from a surface segregation process during the MBE growth. This has been demonstrated on symmetrical structures, and the nominal position of indium was deter-

mined with reference to AlAs films. Furthermore, a novel technique, which, by predeposition of indium, controls the segregation itself in order to build abrupt interfaces in the InGaAs/GaAs system, has been validated.

References

[1] Mo Y.M., Savage D.E., Schwarzentruber B.S. and Legally M.G., Kinetic pathway in Stranski-krastanov growth of Ge on Si (001), *Phys. Rev. lett.* **65** (1990) 1020.

[2] Eaglesham D.J. and Cerullo M., Dislocation-free Stranski-Krastanov growth of Ge on Si (100), *Phys Rev. Lett.* **64** (1993) 1943.

[3] Goldstein L., Glas F., Marzin J.Y., Charasse M.N. and Le Roux G., Growth by molecular beam epitaxy and characterization of InAs/GaAs strained-layer superlattices, *Appl. Phys. Lett.* **47** (1985) 1099.

[4] Houzay F., Guille C., Moison J.M., Henoc P. and Barthe F., First stages of the MBE growth of InAs on (001) GaAs, *J. Crystal Growth* **81** (1987) 67.

[5] Grunthaner F.J., Yen M.Y., Fernandez R., Lee T.C., Madhukar A. and Lewis B.F., *Appl. Phys. Lett.* **46** (1985) 983.

[6] Berger P.R., Chang K., Battacharya P.K. and Singh J., A study of strain-related effects in the molecular beam epitaxy growth of InGaAs on GaAs using reflection high-energy electron diffraction, *J. Vac. Sci. Technol.* **B5** (1987) 1162.

[7] Copel M., Reuter M.C., Kaxiras E. and Tromp R.M., *Phys. Rev. Lett.* **70** (1993) 966.

[8] Grandjean N., Massies J. and Etgens V.T., *Phys. rev. Lett.* **69** (1992) 796.

[9] Choi C.H., Bamett S.A., *Phys. Rev. Lett.* **67** (1991) 2826.

[10] Gerard J.M., Marzin J.Y., Jusserand B., Glas F. and Primot J., *Appl. Phys. Lett.* **54** (1989) 30.

[11] Briones F., Gonzalez L. and Ruiz A., *Appl. Phys.* **49** (1989) 729.

[12] Tamargo M.C., Hull R., Greene L.H., Hayes J.R. and Cho A., *Appl. Phys. Lett.* **46** (1985) 569.

[13] Ohno H., Katsumi R., Takama T. and Hasegawa H., *Jpn. J. Appl. Phys.* **24** (1985) L682.

[14] Massies J., Turto F., Salettes A. and Contour J.P., *J. Cryst. Growth* **80** (1987) 307.

[15] Moison J.M., Guille C., Houzay F., Barthe F. and Van Rompay M., Surface segregation of third-column atoms in group III-V arsenide compounds: ternary alloys and heterostructures, *Phys. Rev.* **B 40** (1989) 6149, and references therein.

[16] Le Goues F.K., Copel M. and Tromp R.M., *Phys. Rev.* **B 42** (1990) 11690.

[17] Gerard J.M., Highly strained InAs/GaAs short period superlattices, in "Condensed Systems of Low Dimensionality", J.L. Beeby Ed., NATO ASI Series B253, Plenum, New York (1991).

[18] Gerard J.M. and Marzin J.Y., Monolayer-scale optical investigation of segregation effects in semiconductor heterostructures, *Phys. Rev.* **B 45** (1992) 6313.

[19] Gerard J.M., High resolution in situ measurement of the surface composition of InGaAs and InAlAs at growth temperature, *J. Crystal Growth* **127** (1993) 981.

[20] Gerard J.M. and Le Roux G., *Appl. Phys. Lett.* **62** (1993) 3452.

[21] Quillec M., Goldstein L., Le Roux G., Burgeat J. and Primot J., *J. Appl. Phys* **55** (1984) 2907.

[22] d'Anterroches C., Marzin J.Y., Le Roux G. and Goldstein L., *J. Crystal Growth* **81** (1987) 121.

[23] Stadelmann P., *Ultramicroscopy* **21** (1987) 131.

[24] Bierwolf R., Hohenstein M., Philipp F., Brandt O., Crook G.E. and Ploog K., *Ultramicroscopy* **49** (1993) 273.

[25] Jouneau P.H., Tardot A., Feuillet G., Mariette H. and Cibert J., *J. Appl. Phys.* **75** (1994) 7310.

[26] Desseaux J., Renault A. and Bourret A., *Phil. Mag.* **35** (1977) 357.

[27] Thoma S. and Cerva H., *Ultramicroscopy* **35** (1991) 77.

[28] Ourmazd A., *J. Cryst. Growth* **98** (1989) 72.

[29] Frank J., *Optik* **38** (1973) 519.

[30] Treacy M., Gibson J.M., *J. Vac. Sci. Techno* **B4** (1986) 1458.

[31] d'Anterroches C., Gerard J.M., Marzin J.Y., NATO ASI series Ed. D. Cherns **203** (1990) 47.

[32] Yen M.Y., Madhukar A., Llewis B.F., Fernandez R., Eng L. and Grunthaner F.J., *Surf. sci.* **174** (1986) 606.

[33] Gerard J.M., d'Anterroches C. and Marzin J.Y., *J. Crystal Growth.* **127** (1993) 536.

[34] Giannini C., Tapfer L., Lagomarsino L., Boulliard J.C., Taccoen A., Capelle B., Ilg M., Brandt O. and Ploog K., Submitted to Phys. Rev. B.